Direct control of magnetic chirality in NdMn$_2$O$_5$ by external electric field

I. A. Zobkalo [1,*] A. N. Matveeva,[1] A. Sazonov,[2] S. N. Barilo,[3] S. V. Shiryaev,[3] B. Pedersen,[4] and V. Hutanu[2,†]

[1]*B.P Konstantinov Petersburg Nuclear Physics Institute, NRC Kurchatov Institute, Gatchina 188300, Russia*
[2]*Institute of Crystallography, RWTH Aachen University and Jülich Centre for Neutron Science (JCNS)*
at Heinz Maier- Leibnitz Zentrum (MLZ), 85747 Garching, Germany
[3]*Scientific-Practical Materials Research Centre NAS of Belarus, Minsk 220072, Belarus*
[4]*Heinz Maier- Leibnitz Zentrum (MLZ), Technische Universität München, 85748 Garching, Germany*

Detailed investigation of the incommensurate magnetic ordering in a single crystal of multiferroic NdMn$_2$O$_5$ has been performed using both nonpolarized and polarized neutron-diffraction techniques. Below $T_N \approx 30.5$ K magnetic Bragg reflections corresponding to the nonchiral-type magnetic structure with propagation vector $\boldsymbol{k}_1 = (0.5\ 0\ k_{z1})$ occurs. Below about 27 K a distorted magnetic modulation with a similar vector k_{z2} occurs, which is attributed to the magnetization of the Nd^{3+} ions by the Mn sublattice. Strong temperature hysteresis in the occurrence of the incommensurate magnetic phases in NdMn$_2$O$_5$ was observed depending on the cooling or heating history of the sample. Below about 20 K the magnetic structure became of a chiral type. From spherical neutron polarimetry measurements, the resulting low-temperature magnetic structure k_{z3} was approximated by the general elliptic helix. The parameters of the magnetic helixlike ellipticity and helical plane orientation in regard to the crystal structure were determined. A reorientation of the helix occurs at an intermediate temperature between 4 and 18 K. A difference between the population of right- and left-handed chiral domains of about 0.2 was observed in the as-grown crystal when cooling without an external electric field. The magnetic chiral ratio can be changed by the application of an external electric field of a few kV/cm, revealing strong magnetoelectric coupling. A linear dependence of the magnetic chirality on the applied electric field in NdMn$_2$O$_5$ was found. The results are discussed within the frame of the antisymmetric superexchange model for Dzyaloshinskii-Moriya interaction.

I. INTRODUCTION

Magnetic multiferroics have attracted increasing scientific interest in the last 15 years. In this class of materials magnetic order induces the long-range polar order and vice versa, thus both order parameters are strongly coupled. A coupling between two ferroic orders can induce novel functional properties that do not exist in either state alone. This fact provides technological interest to such materials, in particular to their potential use in various areas of spintronics, but also in the context of the fundamental understanding of various microscopic mechanisms leading to the magnetoelectric coupling.

Manganite oxides family RMn$_2$O$_5$ (R=rare-earth element) represents a prominent example of multiferroics with an extremely interesting and close relationship between magnetism and ferroelectricity [1–3], including a magnetically induced polarization flop in TmMn$_2$O$_5$ [4], a polarization flip in TbMn$_2$O$_5$, also induced by a magnetic field [1], or electrically induced switching of antiferromagnetic domains in YMn$_2$O$_5$ [5]. The temperature evolution of the magnetic structure of multiferroic RMn$_2$O$_5$ is rather complex, which, in a combination with a variety of magnetoelectric phenomena, makes these compounds extremely attractive from the standpoint of

studying fundamental phenomena of interaction between different order parameters. The intriguing feature of the RMn$_2$O$_5$ family is that compounds with rare-earth ions having a radius smaller than that of Nd^{3+} are multiferroics, while those with a larger radius are not. NdMn$_2$O$_5$ itself, considered to be nonmultiferroic for a long time, is of particular interest as a "borderline" in this series. Especially, only recently observed emergence of the electrical polarization in the magnetically ordered phase of this compound and its much lower value compared to that in another RMn$_2$O$_5$ multiferroics [6], makes it an attractive candidate for the verification of different proposed mechanisms of multiferroicity in this type of materials.

Generally, all members of the RMn$_2$O$_5$ family are considered to be isostructural within the orthorhombic centrosymmetric space group $Pbam$ [7]. This structure consists of octahedra Mn^{4+}O$_6$ edge shared along the c axis and pairs of tetragonal pyramids Mn^{3+}O$_5$ linked to two Mn^{4+}O$_6$ chains. However, there are some indications in the literature about the symmetry lowering in RMn$_2$O$_5$ from $Pbam$ down to $Pb2_1m$ polar group at low temperatures [8–10]. It was reported also that in fact the structure is noncentrosymmetric even at room temperature, and noncentrosymmetric monoclinic space group $Pm(\gamma = 90°)$ was proposed rather than the centrosymmetric one $Pbam$ [11]. In this structure, there are several nearly equivalent superexchange paths between manganese ions that lead to the essential exchange competition, which, in

*Corresponding author: Zobkalo_IA@pnpi.nrcki.ru
†Corresponding author: Vladimir.Hutanu@frm2.tum.de

turn, results in noncollinear magnetic structures and complex magnetic phases [12]. Multiple magnetic ordered phases suggest sophisticated magnetic interaction schemes, so it is reasonable to suppose that several mechanisms could be responsible for the complicated magnetoelectrical behavior in RMn$_2$O$_5$ compounds.

The magnetic order in NdMn$_2$O$_5$ single crystal was studied recently by the neutron scattering [6,13,14]. The magnetic ordering in this compound was found to have features different from those known for other RMn$_2$O$_5$ multiferroics with smaller ion radii. For NdMn$_2$O$_5$ the onset of the long-range magnetic order with incommensurate wave vector $\boldsymbol{k} = (0.5\,0 \sim 0.36)$ is observed at $T_N \approx 30$ K, while for other RMn$_2$O$_5$ multiferroics the transition to magnetically ordered phase takes place at temperatures higher than 40 K. Below 30 K two magnetic phases were reported, their propagation vectors being close to each other: $\boldsymbol{k}_1 = (0.5\,0\,k_{z1})$, $\boldsymbol{k}_2 = (0.5\,0\,k_{z2})$. In Refs. [6,14] it is shown that two propagation vectors merge together at temperature below $T = 15$ K, while in Ref. [13] we show that k_{z1}, k_{z2} components remain separated and increase monotonously with the temperature decrease down to 25 K, then remain constant with values $k_{z1} = 0.384(2)$, $k_{z2} = 0.395(2)$. Two additional transitions were observed at $\sim$20 K and at $\sim$5 K. The latter is connected with Nd^{3+} subsystem alignment with $\boldsymbol{k}_{Nd} = (0.5\,0\,0)$ [14]. The transition at 20 K, related to the ordering of Mn magnetic moments, is of another nature and is of particular interest, since at 20 K the onset of electric polarization in NdMn$_2$O$_5$ single crystal was observed [6]. The most significant issue in the studies of RMn$_2$O$_5$ is the understanding of the microscopic mechanism responsible for the spin-driven ferroelectricity in these compounds. The model of inverse Dzyaloshinskii-Moriya interaction (DMI) works well for magnetic multiferroics in the RMnO$_3$ family, like TbMnO$_3$, DyMnO$_3$. In this model, DMI favors the displacement of O^{2-} ions, which enhances the DMI exchange interaction between noncollinearly ordered spins and breaks the inversion symmetry [15,16]. It is important to note that in RMn$_2$O$_5$ multiferroics ferroelectric polarization was enhanced in the commensurate magnetic phases with magnetic moments close to collinear alignment [2,17]. This provides considerable difficulty in the explanation of the origin of ferroelectric polarization by the inverse DM model. In connection with this, the exchange striction mechanism is used to explain the origin of ferroelectricity [10,12]. This model refers to collinear spin orders, where the symmetric exchange striction causes two nearest ions with parallel spins to move closer to each other, while those with antiparallel spins to move farther. The application of this model to RMn$_2$O$_5$ seems to be reasonable since the antisymmetric exchange is associated with a rather weak spin-orbit coupling. However, from another point of view, the competition of superexchange interactions leads to an exchange-frustrated structure [3], and in such a case, a weak antisymmetric interaction can have a significant impact on the magnetic properties and subsequently on the electric properties of such a system. Apparently, this magnetic frustration is the reason why a considerable number of experimental facts indicate that a significant contribution to a rich set of magnetic phenomena in RMn$_2$O$_5$ is arising due to DMI [18,19]. There are a number of arguments also in favor of multiple microscopic mechanisms of magnetically induced ferroelectricity

in RMn$_2$O$_5$ compounds. NdMn$_2$O$_5$ is an ideal compound for such a study as it belongs to the same multiferroic family, on the one hand, but does not show a commensurate magnetic order on the other. In noncollinear incommensurate magnetic structures of the DMI origin, the direction of spin rotation is fixed by DMI, while in centrosymmetric systems the magnetic energy is independent of the sense of rotation [20]. In order to clarify the role of DMI in formation of magnetic and magnetoelectric properties in RMn$_2$O$_5$ we performed investigations of magnetic chirality and its evolution with the temperature and applied electric field in NdMn$_2$O$_5$. For that we employed the polarized neutrons diffraction. It provides great sensitivity to the direction of the spin rotation in the magnetic structure and allows obtaining information inaccessible by other experimental techniques.

II. EXPERIMENTAL DETAILS

Single crystals of NdMn$_2$O$_5$ were grown by the flux-melt method described in Ref. [21]. The crystal thoroughly characterized in the previous neutron-diffraction investigation [13] was used for the actual experiments. The approximate dimensions of the used sample are $3 \times 4 \times 5$ mm^3 with the longest dimension along the c axis.

The measurements for the crystal-structure refinement were performed at the diffractometer RESI at FRM-II reactor (Heinz Maier-Leibnitz Zentrum, MLZ, Garching, Germany) [22] using neutron wavelength of 1.039 Å. Data collection was made with the image plate position-sensitive 2D detector MAR345. The 2D data reduction was performed using the EVAL-14 suite [23].

Magnetic neutron studies were performed at diffractometer POLI at MLZ [24,25], which permits measurements both in unpolarized and polarized diffraction modes using the same neutron wavelength. Nonpolarized diffraction using variably double-focused Si (311) monochromator and wavelength of 1.15 Å, resulting in high-intensity neutron flux of more than 10^7n(cm^2 s)$^{-1}$ with high resolution, was employed in order to study the thermal evolution of the magnetic Bragg reflections in NdMn$_2$O$_5$.

For the polarized neutron diffraction, we used the technique of spherical neutron polarimetry (SNP). It is implemented on POLI using the third-generation zero-field Cryogenic Polarization Analysis Device CRYOPAD [26]. Both neutron polarization and analysis are performed using ^{3}He spin filters. Such configuration is very efficient for short-wavelength neutrons from the point of view of a good resolution and a high flux of the polarized neutrons on the sample position, superior to the previous investigations. At the same time, because the polarizing (analyzing) efficiency of the filters relaxes (decreases) with time, that represents a main drawback of the technique. The corrections should be done to the data, which may lead to some decrease in the statistical accuracy of the measurement. The additional corrections were performed according to calculations described in Ref. [27]. Standard SNP axis convention was applied for the polarization analysis: $\boldsymbol{x}$ direction coincides with the scattering vector $\boldsymbol{q}$, $\boldsymbol{y}$ direction lies in the scattering plane and is perpendicular to $\boldsymbol{x}$ and $\boldsymbol{z}$ axis is oriented vertically, thus forming a right-handed Cartesian coordinate system.
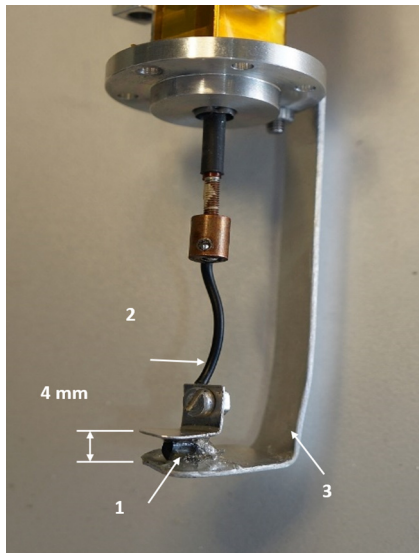
FIG. 1. $NdMn_2O_5$ single-crystal sample (1) between two Al electrodes; (2)–isolated high-voltage contact and (3)–ground; on the sample rod of FRM II close-cycle refrigerator able to control temperature between 3.8 and 325 K with the precision of better than 0.1 K.

During the experiment with polarized neutrons, the crystal b axis was oriented vertically, a and c axes were lying in the horizontal scattering plane. In this way, the magnetic satellites of type $\boldsymbol{k} = (k_x\ 0\ k_z)$ can be reached. For the measurements with the electric field, the crystal was mounted on a sample rod of the cryostat, between the electrodes built from aluminum plates as shown in Fig. 1. The electric field was applied in a vertical direction along the b axis. The sample was placed into a standard FRM-II type top-loading cryostat. The essentials of measurements with high electric fields in cryogenic environments consist of fine-tuning the pressure of helium exchange gas continuously on a thin line, where it is possible to apply several kV/mm without an electric breakdown while maintaining the necessary temperature control of the sample. Prior to the experiment, a reliable setup for *in situ* pressure control and regulation within the cryostat has been developed and calibrated. In this way, an electric voltage up to 5 kV (corresponding to maximum 12.5 kV/cm electric field in the sample) could be applied during the experiment without an electric breakdown. The power-supply device FUG HCB 20M-1000 has been used for high-voltage generation and high-precision digital multimeter FLUKE 8846A for the current monitoring in order to avoid the breakdowns.

III. EXPERIMENTAL RESULTS

A. Crystal-structure refinement

For the crystal-structure refinement, the datasets were collected at three temperatures–300, 24, and 6 K. The observed nuclear reflections were successfully indexed in the *Pbam* space group and we did not observe superstructure reflections that should indicate that the crystal symmetry is lower than *Pbam*. But, we also can suppose that this could be connected with the extremely low intensity of those reflections, as it was observed in Ref. [11]. The structural refinement was then

TABLE I. Crystal-structure parameters obtained within *Pbam* space group.

Atom	X	Y	Z
300 K ($a = 7.4940\,\text{Å}$, $b = 8.6071\,\text{Å}$, $c = 5.6934\,\text{Å}$			
Nd	0.1421(3)	0.1732(4)	0
Mn^{4+}	0	0.5	0.2556(8)
Mn^{3+}	0.4114(7)	0.3539(7)	0.5
O1	0	0	0.2717(5)
O2	0.1579(5)	0.4482(6)	0
O3	0.1520(5)	0.4366(5)	0.5
O4	0.4023(3)	0.2070(4)	0.2497(4)
24 K ($a = 7.4871\,\text{Å}$, $b = 8.6293\,\text{Å}$, $c = 5.7083\,\text{Å}$)			
Nd	0.1424(6)	0.1724(5)	0
Mn^{4+}	0	0.5	0.257(1)
Mn^{3+}	0.411(1)	0.354(1)	0.5
O1	0	0	0.276(1)
O2	0.1588(8)	0.4482(6)	0
O3	0.1514(8)	0.4366(6)	0.5
O4	0.4040(5)	0.2050(5)	0.2485(7)
6 K ($a = 7.5135\,\text{Å}$, $b = 8.6328\,\text{Å}$, $c = 5.7320\,\text{Å}$)			
Nd	0.1436(7)	0.1722(6)	0
Mn^{4+}	0	0.5	0.255(1)
Mn^{3+}	0.413(1)	0.355(1)	0.5
O1	0	0	0.277(1)
O2	0.161(1)	0.4501(7)	0
O3	0.1507(9)	0.4353(7)	0.5
O4	0.4038(6)	0.2059(5)	0.2483(9)

performed with the FULLPROF suite software [28]. The results obtained within the *Pbam* space group are in good agreement with those reported previously at 300 K [6,7] and are presented in Table I. The same datasets were then used for the refinement within the *Pm* space group, but the enhancement of the fit quality was negligible by the significantly increasing number of fitting parameters, which does not permit us to make the definite decision in favor of lower symmetry group.

B. Temperature evolution of the magnetic order by nonpolarized neutron diffraction

In order to identify the magnetic Bragg reflections from different magnetic phases for the polarized-neutron investigation on POLI, we first performed a nonpolarized temperature-dependent neutron-diffraction study using the same sample, instrument settings, and beam parameters as for the subsequent polarized experiment.

The onset of magnetic ordering was observed at about $T_N \sim 30.5$ K in accordance with previous studies [6,13,14]. Below this temperature the magnetic satellites corresponding to the incommensurate propagation vectors $\boldsymbol{k}_1 = (0.5\ 0\ k_z)$, $\boldsymbol{k}_2 = -\boldsymbol{k}_1 = (0.5\ 0\ -k_z)$, $k_z = 0.361(4)$ appear (Fig. 2). If fitted with one Gaussian peak, the value of k_z increases smoothly from 0.361(1) to 0.3967(1) with the temperature decrease from 30.5 K down to $\sim$10 K [Fig. 3(a)]. Below that lock-in temperature the propagation vector component k_z of 0.3967(1) does not change any more down to 4 K. When heated, the lock-in value for k_z remains constant up to $\sim$20 K showing a significant temperature hysteresis and
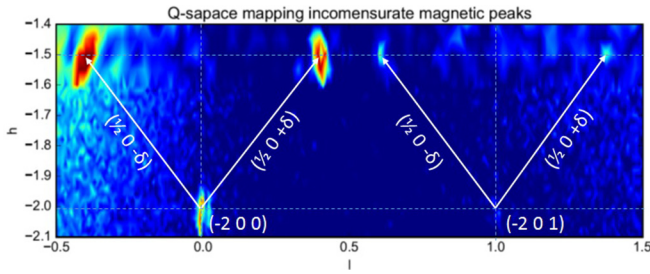
FIG. 2. Q-space mapping of incommensurate magnetic Bragg satellites with propagation vectors $\pm \boldsymbol{k} = (1/2\,0 \pm k_z)$ in NdMn$_2$O$_5$ at 5 K.

decreases smoothly with steeper slope toward higher temperatures, reaching almost the same values as by cooling at about 30 K [Fig. 3(a)]. Hysteretic behavior between cooling and heating in the same temperature region has been reported for the dielectric permittivity in NdMn$_2$O$_5$ powders [6], which combined with our data suggests a possible coupling between magnetic and electric properties. Figure 3(b)
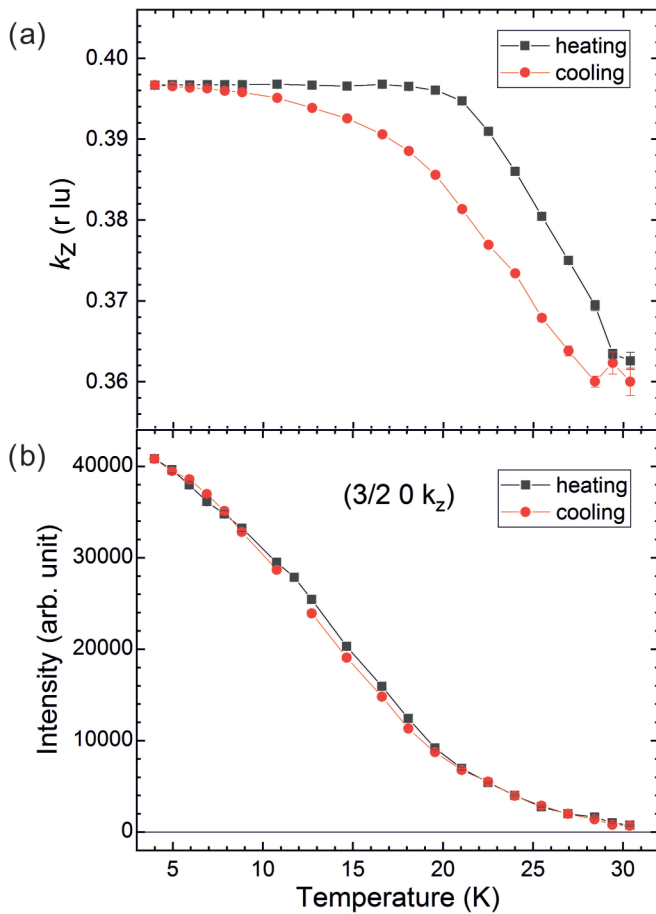

FIG. 3. Temperature dependence of (a) the k_z component of magnetic propagation vectors $\boldsymbol{k}_{1,2}$ and (b) the integrated intensity of the magnetic reflection $(2\,0\,0)^{-k2}$. Both (a) and (b) are plotted based on the fitting of magnetic reflection with one Gaussian peak. Where not visible, the error bars are smaller than the symbols. Lines are guides for the eyes.

shows the temperature evolution of the integrated intensity of the observed magnetic satellite $(2\,0\,0)^{-k2}$ fitted by one Gaussian peak on cooling and heating. Slight temperature hysteresis is observable also for the intensity, however in another temperature region comparing to the thermal evolution of k_z value. The hysteresis is observed between 10 and 21 K. Above that latter temperature, the change in peak intensity is exactly the same when cooled or heated. A pronounced change in the slope of the thermal evolution of the magnetic peak intensity is observed at about the same temperature ~ 21 K. This temperature is of special interest as it is the temperature, where the emergence of the electric polarization in NdMn$_2$O$_5$ is reported [6]. Similar anomaly in the integrated intensities at ~ 20 K of other magnetic satellites, e.g., $(0\,1\,0)^{+k1}$, $(2\,1\,0)^{-k2}$, $(0\,0\,0)^{+k1}$, and $(0\,1\,2)^{+k2}$ was observed also in the previous studies [6,13]. In Ref. [6] three different types of the magnetic reflections, in regard to the thermal evolution, were reported: those occurring at about 30 K and monotonously increasing down to the lower temperatures, e.g., $(0\,1\,0)^{+k1}$. Others, like those mentioned above, also occurred at about 30 K, slowly increased down to about 20 K, increasing sharply at lower temperatures. The third type only appears below 20 K and then continuously increases with the temperature lowering, e.g., $(0\,0\,1)^{+k2}$. Such complex behavior has been interpreted as the presence of different incommensurate magnetic phases with slightly different magnetic propagation vectors k_{z1} and k_{z2}, which may coexist in certain temperature regions [6,13,14]. The authors of Refs. [6,14] based on the measurements of neutron-powder diffraction and tiny single crystals proposed a physical picture where between 30 and 15 K there is an incommensurate phase called ICM1 with the coexistence of two slightly different k_{z1} and k_{z2} incommensurate modulations and below 15 K those modulations merge into one structure with k_{z2}, called ICM2. The authors of Ref. [13] based on the single-crystal diffraction suggest the coexistence of the k_{z1} and k_{z2} incommensurate modulations for all temperatures between 30 and 2 K, k_{z1} being a dominant magnetic phase in the region 30-20 K and k_{z2} the main magnetic phase at temperatures below ~ 21 K. The presence of multiple phases with close $\boldsymbol{k}$ vectors should be reflected also in our data. It is worth mentioning that a hot-neutron single-crystal diffractometer is not the best instrument to study the tiny splitting between two magnetic satellites in low-q region; nevertheless, optimizing the detector slits width and monochromator focusing, a certain optimization in the resolution may be reached. Figure 4 shows the temperature dependence of the width of the magnetic satellite $(2\,0\,0)^{-k2}$ resulting from the fit with one Gaussian peak when cooled or heated. The resolution limit of the instrument in this setup was of about 0.012 r.l.u. Two main features can be derived from these results. (A) Even at low temperature (< 10 K), where magnetic satellite does not change with temperature anymore, the absolute value of the peak width full width at half maximum (FWHM) = 0.0168(2) is significantly higher than the resolution of the instrument. This observation is in a good agreement with results reported for powder peaks in Ref. [6] and may suggest either broadening of the peak due to some disorder in the magnetic structure or still the presence of the two very close k_z structures, as suggested
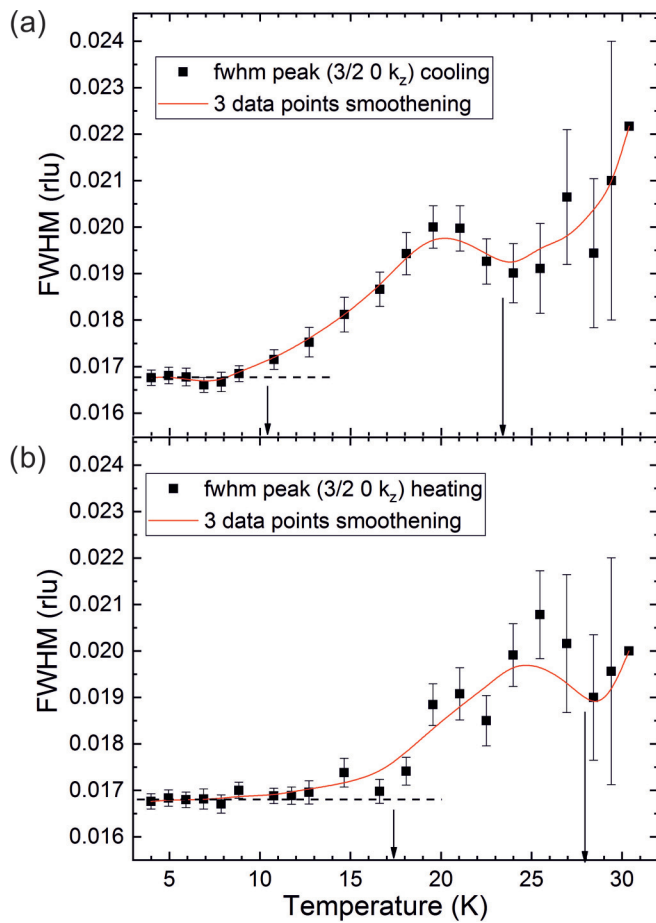
FIG. 4. Temperature dependence of the FWHM for the magnetic Bragg reflection $(2\,0\,0)^{-k2}$ as obtained from the fit with one Gaussian peak, (a) by cooling and (b) by heating. Data points are presented by the black squares; the red lines are the smoothening function by three neighboring points applied to the data as a guide for the eyes. The black arrows indicate the temperature region where an "intermediate" magnetic phase with k_{z2} is supposed to exist (see main text for more details).

FIG. 5. Temperature dependence of the magnetic Bragg reflection $(2\,0\,0)^{+k\mathrm{Nd}}$ by heating with commensurate propagation vector $k_{\mathrm{Nd}} = (1/2\,0\,0)$, associated with spontaneous ordering of the Nd^{3+} magnetic sublattice.

in Ref. [13], with the only difference that they should be of the similar magnitude. (B) The peak broadening (up to twice the instrument resolution limit) is a clear indication of the presence of additional magnetic phases. Depending on the cooling or heating process, the broadening sets at different temperatures resembling somehow the hysteresis behavior observed for the peak positions and intensities shown in Fig. 3. Close inspection of the results of high-resolution powder diffraction from Fig. 6 in Ref. [6] reveals that indeed the primary magnetic phase k_{z1} occurring at about 30 K does not persist down to the very low temperature, but rather down to ∼22 K only; then, an additional phase with close k_{z2} appears at about 26 K and persists down to ∼12 K. This phase can be easily identified by the presence of the 3^*k_{z2} modulation in that temperature region only, as it is seen in Fig. 6 in Ref. [6]. And finally, at about 21 K a third incommensurate phase with k_{z3} appears, which does not change down to the lowest temperature studied. It is not clear whether results presented in Fig. 6 of Ref. [6] are measured in the heating or cooling mode; however, comparing this physical
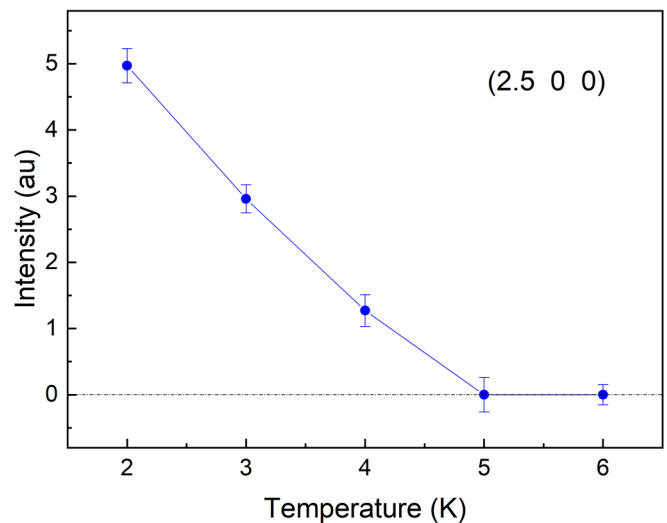
picture to our results a clear similarity to our results in the cooling mode could be identified. Thus, in certain temperature regions different magnetic phases may coexist, like k_{z1} and k_{z2} between 27 and 23 K and k_{z2} and k_{z3} between 26 and 11 K by cooling, leading to the observed peak broadenings. The observed hysteresis in this scenario may be related to the formation of the intermediate k_{z2} structure. When cooled, Mn magnetic sublattice, which orders at higher temperatures, influences in some way (polarizes) the Nd magnetic sublattice. This results in the nonsinusoidal modulated structure k_{z2} and another modulation k_{z3}. At temperatures close to 5 K, Nd orders spontaneously resulting in the independent magnetic order with commensurate propagation vector $k_{\mathrm{Nd}} = (1/2\,0\,0)$ in good agreement with previous results [6,14]. Figure 5 shows the observed temperature dependence of magnetic peak $(2\,0\,0)^{+k\mathrm{N}d}$. Both Mn magnetic sublattice with k_{z3} and Nd sublattice with k_{Nd} coexist at temperatures below 5 K. While heated, an inverse process of the magnetic influencing may be suggested: the Nd ordered subsystem "polarizes" the Mn sublattice in a way that k_{z3} is maintained up to the higher temperatures and intermediate k_{z2} phase occurs later and disappears quicker by heating toward k_{z1} phase. This scenario well resembles the slow change of the k_z when cooled and steep change when heated observed in Fig. 3. The same model is applicable to the consideration of the peak-width evolution in Fig. 4, denoting some "flexibility" in the occurrence of the phase k_{z2} depending on cooling or heating sample history. Two transition temperatures for the magnetic ordering of Nd in NdMn$_2$O$_5$ have been reported recently from the splitting of crystal-fields levels [29]. According to this study, at 28 K ground-state Kramers doublet splits into two sublevels. This splitting sharply increases below ∼18 K and reaches a maximum at 4.5 K. Such behavior resembles fairly well the thermal evolution of the magnetic structure observed within this study in the heating mode, denoting the influence of the Nd magnetic moment on the magnetic structure of the Mn sublattice.

C. Magnetic structure in zero electric field by spherical neutron polarimetry

The SNP technique allows measuring the relationship between the polarization of the incident and scattered neutron beams. It allows distinguishing between polarization rotation occurring upon scattering from lattice of the ordered magnetic moments and depolarization due to the presence of the magnetic domains. The experimental quantities obtained in SNP experiment for each Bragg reflection are the components P_{ij} of the 3×3 polarization matrix P of the type $\mathcal{P}_{ij} = \frac{I_{ij}^+ - I_{ij}^-}{I_{ij}^+ + I_{ij}^-}$, where the indices i, j refer to one of the orthogonal directions x, y, z of the initial and final (scattered from the sample) polarization, correspondingly. The first subscript corresponds to the direction of the initial polarization vector, while the second is the direction of analysis. I is the measured intensity with polarization parallel "$+$" and antiparallel "$-$" to the initial polarization direction i. In the general case in all elements $\mathcal{P}_{ij}$ the contributions from nuclear and magnetic scattering exists, some of them containing also nuclear-magnetic interference and chiral scattering terms. A more detailed description of the SNP technique can be found elsewhere [30].

Considering magnetic ordering in a crystal as a plane elliptical helix, in a general case one can describe it by the following expression:

$$M(r_n) = u\mu_u \cos(r_n \cdot k) + v\mu_v \sin(r_n \cdot k), \quad (1)$$

where u, v are unit vectors, orthogonal to each other; μ_u, μ_v are corresponding amplitudes; r_n is a cell position; helix vector $m = [u \times v]$, and k is helicoid propagation vector. The diffraction on the incommensurate magnetic structure produces pure magnetic reflections, free from nuclear contribution. In the SNP mode we measured only those elements of polarization matrix, which will give most valuable information in a case of incommensurate magnetic structure, namely elliptic parameters $\mathcal{P}_{yy}$ and $\mathcal{P}_{zz}$ and chiral parameters $\mathcal{P}_{yx}$ and $\mathcal{P}_{zx}$ as well as scaling parameter $\mathcal{P}_{xx}$, denoting total magnetic scattering, which should be equal to -1 for purely magnetic reflection [30]. In this case terms of interest can be expressed as [19]

$$\mathcal{P}_{yy} = -\mathcal{P}_{zz} \sim \frac{\mu_u^2\cos^2\beta - \mu_v^2}{\mu_u^2\cos^2\beta + \mu_v^2} = \frac{R^2\cos^2\beta - 1}{R^2\cos^2\beta + 1}, \quad (2)$$

$$\mathcal{P}_{yx} = \mathcal{P}_{zx} \sim \frac{2(1 - 2n_r)\mu_u\mu_v}{\mu_u^2 + \mu_v^2} = \frac{2(1 - 2n_r)R\cos\beta}{R^2\cos^2\beta + 1}. \quad (3)$$

In these expressions v is considered to be directed vertically, u horizontally, β is the angle between the helix vector m and the scattering vector q (Fig. 6), $R = \mu_u/\mu_v$ is ellipticity; n_r is a portion of "right-hand" helices in crystal; $n_l = 1 - n_r$ is a portion of "left-hand" helices. Thus, the overall relative chirality for the k_n structure could be denoted as $Ck_n = n_l(k_n) - n_r(k_n)$.

It should be noted that because of low intensities of scattering from phase k_{z1} and k_{z2} above 22 K [Fig. 3(b)] the measurements of polarization matrix elements were performed in a heating mode only for satellites from phase k_{z3} at 4 K and later at 18 and 20 K where according to Fig. 3(a) and Fig. 4 the influence of the k_{z2} phase could be observed. The measured
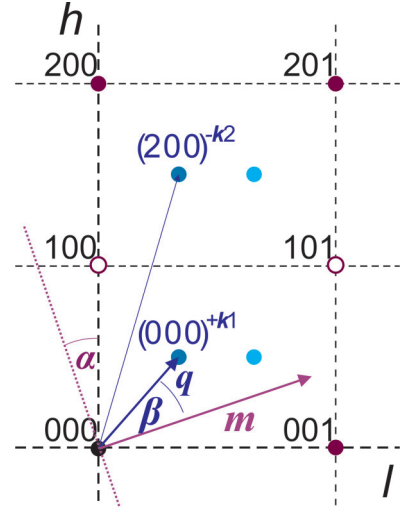

FIG. 6. Scheme of the consideration of directions in reciprocal space.

polarization matrix elements for two different magnetic Bragg satellites with $+k$ and $-k$ vectors and different angles β (see Fig. 6) measured at 4, 18, and 20 K are shown in Table II.

The presence of the nonzero chiral parameters $\mathcal{P}_{yx}$ and $\mathcal{P}_{zx}$ of the same sign is clear direct evidence that the underlying incommensurate magnetic structure at 4 K is of the chiral type (cycloidal or helical order) and not a flat spin-wave modulation as previously suggested [6]. The nonzero value of these components gives evidence about the nonequal population of the domains with the right and left chiral handedness. Using the data at 4 K from Table I the calculation gives an estimation for chirality in k_{z3} phase $Ck_{z3} = 0.20(2)$. At 18 K one still observes some nonzero chiral terms, but statistics is not as good because of the low satellite intensity in comparison with the 4 K. However, the fact that both $\mathcal{P}_{yx}$ and $\mathcal{P}_{zx}$ components are of the same sign for both reflections and their sign is the same as for 4 K may serve as an indication that at 18 K the chiral magnetic phase k_{z3} is still persisting, also keeping the same type of imbalance between two different chiral handedness. At 20 K the chiral components $\mathcal{P}_{yx}$ and $\mathcal{P}_{zx}$ could not be measured any more reliably. This cannot be explained solely by decreasing statistics, and is an intrinsic treasure of the changing magnetic structure.

The elliptic parameters $\mathcal{P}_{yy}$ and $\mathcal{P}_{zz}$ for both $(2\,0\,0)^{-k2}$ and $(0\,0\,0)^{+k1}$ reflections in Table I also change with temperature. The more pronounced effect takes place for $(0\,0\,0)^{+k1}$ satellite, where $\mathcal{P}_{yy}$ and $\mathcal{P}_{zz}$ change their signs between 4 and 18 K. This is clear evidence that orientation of the magnetic moments in k_{z3} structure changes significantly between those temperatures while heated. Comparing this result with the temperature evolution of the peak width from Fig. 4(b), this reorientation may be ascribed to the emerging additional phase called k_{z2} at an intermediate temperature. No orientation change is observable between 18 and 20 K by further temperature increase. Assuming helical-type magnetic structure and using Eq. (2) it is possible to calculate resulting magnetic helix parameters like ellipticity R and helix plane orientation. Obtained in this way the angle α between the magnetic helix plane and crystallographic ab plane for the k_{z3} magnetic

TABLE II. Polarization matrix elements for magnetic satellites $(2\,0\,0)^{-k2}$ and $(0\,0\,0)^{+k1}$ measured at different temperatures and zero electric field.

	$(2\,0\,0)^{-k2}$			$(0\,0\,0)^{+k1}$		
4 K	x	y	z	x	y	z
x	$-1.041(14)$			$-0.98(4)$		
y	$-0.19(5)$	$-0.316(13)$		$-0.20(2)$	$-0.20(2)$	
z	$-0.08(4)$		$0.292(14)$	$-0.19(2)$		$0.19(2)$
		$(2\,0\,0)^{-k2}$			$(0\,0\,0)^{+k1}$	
18 K	x	y	z	x	y	z
x	$-0.98(7)$			$-0.98(10)$		
y	$-0.05(7)$	$-0.580(22)$		$-0.19(5)$	$0.35(2)$	
z	$-0.09(6)$		$0.584(24)$	$-0.06(5)$		$-0.36(2)$
		$(2\,0\,0)^{-k2}$			$(0\,0\,0)^{+k1}$	
20 K	x	y	z	x	y	z
x	$-1.036(23)$			$-0.98(7)$		
y		$-0.728(21)$				
z			$0.721(21)$			$-0.53(10)$

structure is 22.2(3.2)° at 4 K. At higher temperatures a helix changes its orientation: the major and minor elliptic axes are swept and the angle between the helix plane to the *ab* plane is tilted to the $\alpha = -4.7(4)°$ at 18 K, and $\alpha = -10.4(1.2)°$ at 20 K, respectively. The ellipticity of the magnetic structure R, denoting the ratio between major and minor axes of the helix in the plane, changes also with temperature. $R = 1$ would correspond to a perfectly circular helix. Deviations from 1 denote distortions (elongations) of the ellipse. Calculated for different temperatures, R values are 0.77(13), 2.16(11), and 3.06(50) for 4, 18, and 20 K, respectively, showing clear shrinking (elongation) of the helix toward the transition temperature around 21 K, where the chiral character disappeared (as shown in the next section), and plane spin-density wave modulation is formed. The schematic representation of such transformation from chiral helical structure to nonchiral collinear spin-wave one is shown in Fig. 7.

D. Magnetic chirality under applied electric field by polarized neutron diffraction

Because of low intensities of magnetic satellites, for the study of electric-field dependence on chiral scattering, in order to increase statistics, we applied the technique of polarized neutron diffraction without the analysis of scattered beam polarization. In this case the loss of neutrons due to the limited transmission of the analyzer is avoided, while chiral scattering can be unambiguously detected. The expression for the intensity of polarized neutrons, scattered on a magnetic satellite from helical structure [31], can be written in the simplified form as

$$I_x^{\pm} \sim \boldsymbol{M}_{\perp}\boldsymbol{M}_{\perp}^* \mp iCk_n\,(\boldsymbol{M}_{\perp}\times\boldsymbol{M}_{\perp}^*\,)_x, \qquad (4)$$

where $\boldsymbol{M}_{\perp}$ is effective magnetic moment participating in scattering process, perpendicular to scattering vector $\boldsymbol{q}$:

$$\boldsymbol{M}_{\perp} = \boldsymbol{q}\times(\boldsymbol{M}\times\boldsymbol{q}), \qquad (5)$$

and $I_x^{\pm}$ is intensity of scattered neutrons with initial neutron polarization along $\boldsymbol{x}$ axis $(+)$ or opposite to it $(-)$ and the $\boldsymbol{x}$ axis is directed along the scattering vector $\boldsymbol{q}$. In this way, total magnetic intensity $I_M = (I_x^{+} + I_x^{-})/2$ as well as the pure chiral part of the magnetic scattering $I_{Ch} = (I_x^{+} - I_x^{-})/2$ can be obtained if $Ck_n \neq 0$. At the temperature 4 K the results for chirality obtained by this technique were compared with those from SNP for the consistency.
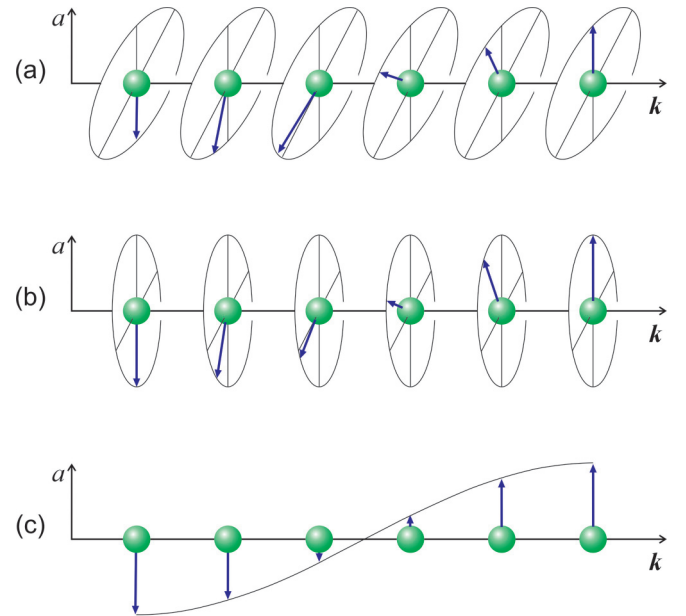

FIG. 7. Schematic representation of the transformation of an elliptical spiral into a transverse spin-wave modulation in NdMn$_2$O$_5$ with temperature increase: (a) almost-circular helix with minor axis along *a*–corresponding to configuration at 4 K, (b) transformed (elongated) helix with major axis along *a* at 18–20 K, and (c) plane spin-wave modulation presumably at $T > 21$ K.
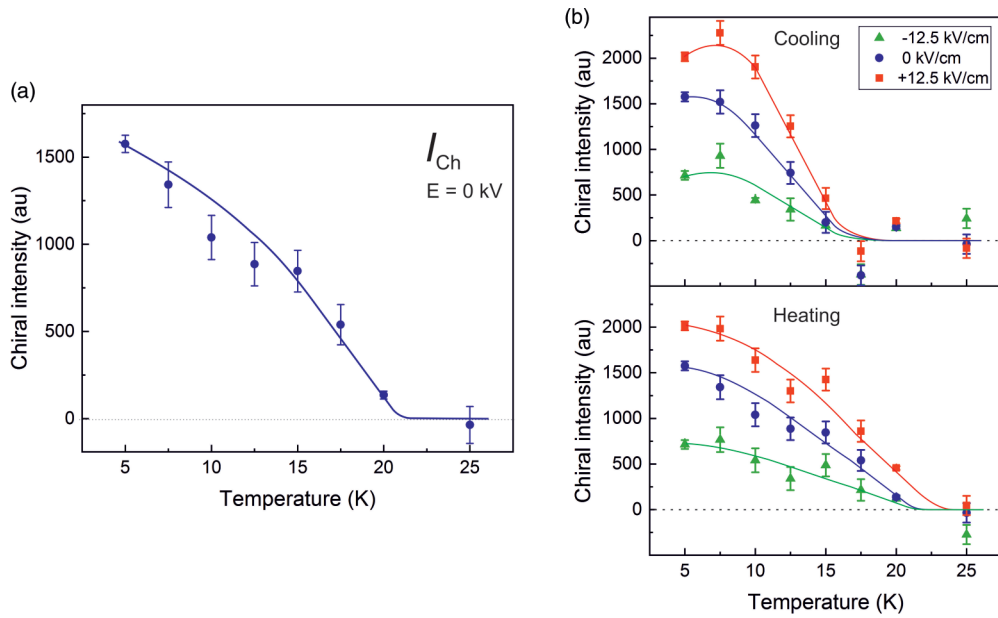
FIG. 8. (a) Temperature evolution of chiral scattering I_{Ch}, measured on satellite $(2\,0\,0)^{-k2}$ in heating mode without electric field. (b) The temperature evolution of chiral scattering I_{Ch} on the same satellite as function of electric field on cooling and heating mode. Solid lines are guides for eyes.

The temperature evolution of chiral scattering, measured on magnetic satellite $(2\,0\,0)^{-k2}$ without electric field, is shown in Fig. 8(a). It is easy to see that the chiral scattering appears below $T \approx 21\,\text{K}$. This means that below $T_{\text{N}} \approx 30\,\text{K}$ in NdMn$_2$O$_5$ a nonchiral incommensurate magnetic ordering emerges, while at $T_{\text{Ch}} \approx 21\,\text{K}$ the transition to chiral structure takes place. The crossover observed in the temperature dependence of the integrated intensities of magnetic satellites reflect this transition and the proposed k_{z3} magnetic structure is of chiral nature. The existence of the nonchiral spin-wave modulation phase in the intermediate temperature region between paramagnetic and ferroelectric phases is observed also for type-II multiferroic compounds—members of perovskite manganites family RMnO$_3$ with R = Tb, Dy [32–34] as well as some doped RMn$_2$O$_5$ family representatives like YMn^{4+}(Mn$_{0.88}$Ga$_{0.12}$)$^{3+}$O$_5$ [18].

In order to study the effect of the electric field on the magnetic properties of NdMn$_2$O$_5$ we first applied $+5$-kV voltage along the b direction (which yields electric field $+12.5\,\text{kV/cm}$) at a fixed low temperature of 4 K while the sample was cooled without electric field. This action had no measurable effect on the magnetic satellites. Then the measurements in the field-cooled (FC) mode were performed in the following way: crystal was warmed up to the temperature of 40 K, i.e., well above the transition temperature $T_{\text{N}} = 30.5\,\text{K}$, then the voltage was applied and the sample cooled down to 5 K under the applied electric field. The sample was warmed up back to 40 K under the same field, then the voltage value was changed. The following sequence of applied fields was used: $+5\,\text{kV}$ ($+12.5\,\text{kV/cm}$), $+2.5\,\text{kV}$ ($+6.25\,\text{kV/cm}$), $0\,\text{kV}$, $-2.5\,\text{kV}$ ($-6.25\,\text{kV/cm}$), $-5\,\text{kV}$ ($-12.5\,\text{kV/cm}$). The intensities I_x^+ and I_x^- were measured for selected magnetic satellites while cooling/heating under field at temperatures of 25, 20, and then with 2.5 K step by temperature lowering down to 5 K, and then while heating at the same temper-

ature points. The results of such measurements for satellite $(2\,0\,0)^{-k2}$ are presented in Fig. 8(b). The application of the electric field in FC mode does not change T_{Ch} for the same cooling/heating mode, while the intensity of the chiral scattering changes considerably. Depending on the field polarity certain chiral domains will be favored or suppressed. The behavior seems to be symmetric in regard to the preexisting imbalance of domains with two-handedness in the sample at zero field. Some temperature hysteresis of few Kelvin for T_{Ch} around 20 K depending on the heating or cooling mode was observed for chiral scattering. One should point out that the application of electric field (FC mode) did not change elliptic terms within the accuracy of the measurements. In Fig. 9 the chirality Ck_3 is plotted as a function of the applied electric
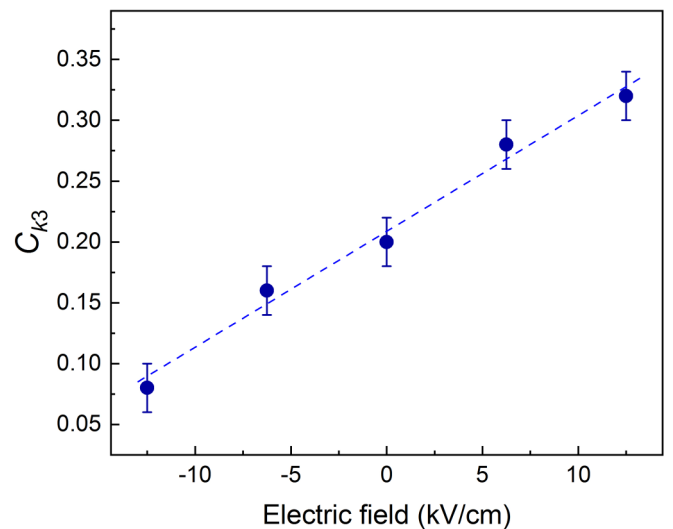

FIG. 9. Electric-field dependence of magnetic chirality Ck_3 measured at 4 K in FC mode.
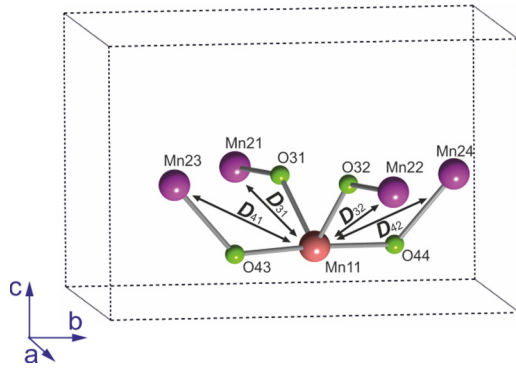
FIG. 10. Exchange paths for $Mn^{4+} - Mn^{3+}$ pairs in RMn_2O_5 considering monoclinic space group Pm.

field. This pretty much linear behavior is observable for both phases. This is different comparing to the situation observed in $TbMn_2O_5$ [19], where similar measurements reveal a kind of hysteretic behavior in the chirality vs electric-field phase diagram. This result denotes weaker pinning of the chiral domain walls to the crystal frame in $NdMn_2O_5$ than in the case of $TbMn_2O_5$.

IV. DISCUSSION

The emergence of the chiral scattering was observed at the temperature T_{Ch} which coincides with T_{CE} where ferroelectric polarization starts to occur. This leads us to the suggestion that namely the chiral magnetic structure is the origin of the ferroelectric polarization in $NdMn_2O_5$. Here it is appropriate to mention that antisymmetric DMI determines the direction of rotation of the spirals in the chiral magnetic structures [20]. The possibility of the existence of nonzero integral DMI in RMn_2O_5 was discussed previously in YMn_2O_5 [18] and recently for $TbMn_2O_5$ [19]. The considerations use a qualitative model based on the antisymmetric superexchange through an anion [34,35] taking into account the crystal symmetry of the noncentrosymmetric space group Pm rather than $Pbam$ [11]. Apparently, the argumentation made there for $TbMn_2O_5$ is applicable also for $NdMn_2O_5$, which we repeat briefly here.

The antisymmetric superexchange through an anion can be expressed as [35,36]

$$V_{DM} = D[\mathbf{S}_1 \times \mathbf{S}_2], \quad (6)$$

where $\boldsymbol{D} = d(\theta)[\mathbf{R}_1 \times \mathbf{R}_2]$ is Dzyaloshinskii vector in this case. $\mathbf{R}_1$, $\mathbf{R}_2$ are unit vectors, connecting magnetic ions with anion. Their vector product fixes the direction of $\boldsymbol{D}$. The antisymmetric exchange parameter $d(\theta)$ depends in a rather complex manner on the local anisotropy of metal ion, on the particularities of metal–ligand bonds, and its sign depends on the bond angle θ [33]. The sign of the antisymmetric parameter $d(\theta)$ changes at a critical angle θ_k which is characteristic for each particular interacting cation-anion group. Within monoclinic space group Pm [11] the four pairs of interacting manganese ions $Mn^{3+} - Mn^{4+}$ will give nonzero total interacting vector $\boldsymbol{D}$ (Fig. 10). For these pairs the Heisenberg exchange interactions are usually considered as J_3 and J_4. By the analogy, we will designate antisymmetric interactions under consideration as $\boldsymbol{D}_3$ and $\boldsymbol{D}_4$. In the case of noncentrosymmetric space group Pm there will be four inequivalent

interaction $\boldsymbol{D}_{31}$, $\boldsymbol{D}_{32}$ and $\boldsymbol{D}_{41}$, $\boldsymbol{D}_{42}$. The bond angles on the regarded exchange paths are close to 130°, which is a critical superexchange value according to Goodenough-Kanamori-Andersen rules [37].

It was shown for RMn_2O_5 [38] that oxygen locations relative to those of Mn^{3+} and Mn^{4+} ions play an important role in the determination of the magnetic properties. In this situation, a tiny deviation in anion position could cause a sharp change of the magnetic interaction [38]. This change should refer not only to the symmetric exchange but to the antisymmetric one as well. The comparison of the exchange bonds between the manganese ions as shown in Fig. 10 for $NdMn_2O_5$ and $TbMn_2O_5$ can be done based on the $Pbam$ crystal structure, since, to our best knowledge, there are no exact data on the oxygen positions in $NdMn_2O_5$ and $TbMn_2O_5$ within space group Pm available. According to data from Ref. [7] the Mn11–O43–Mn23 and Mn11–O44–Mn24 angles and bonds corresponding to $\boldsymbol{D}_{41}$, $\boldsymbol{D}_{42}$ are similar for the both compounds, whereas for the pairs Mn11–O31–Mn21 and Mn11–O32–Mn22 (defining $\boldsymbol{D}_{31}$, $\boldsymbol{D}_{32}$) they are different. In $NdMn_2O_5$ there is a noticeable displacement of the oxygen ions O31, O32 away from the Mn11 (Mn^{4+}) toward the ions Mn21 and Mn22 (Mn^{3+}), respectively, comparing to $TbMn_2O_5$. The bond length Mn1–O3 is 2.076 Å for $NdMn_2O_5$ and 2.021 Å for $TbMn_2O_5$, respectively [7]. In both cases the angles are very close to the critical value of 132.4°–132.5°.

Comparing the positions for the oxygen ions, for space group Pm [11] with those for $Pbam$ [7] one can see that oxygen ions involved in DM interaction under our consideration O31, O32, O43, O44 have the largest polar displacements. Being the most "mobile" in this structure, these ions (or some of them) could undergo displacements under the influence of the electric field. These displacements provoke the change in the sign of the antisymmetric exchange parameter $d(\theta)$ in some domains, thus favoring predominant formation of the domains with certain handedness of the helices.

According to the obtained results of the chirality evolution under the applied electrical field we can suppose that geometrical arrangement of the considered superexchange in $NdMn_2O_5$ is closer to the critical one than that of $TbMn_2O_5$, and therefore $NdMn_2O_5$ demonstrates less rigid chirality-to-lattice coupling. Crystal structure of RMn_2O_5 provides multiple competing magnetic interactions, and correspondingly it is exchange frustrated, which yields the competing magnetic ground states. For rare-earth ions with the ion radius lower than that of Nd^{3+}, the ground state with commensurate structure, characterized by $\boldsymbol{k} = (0.5\ 0\ 0.25)$, becomes favorable in some temperature region, which is not the case for $NdMn_2O_5$. At the same time the spiral spin structure is still preserved in this commensurate phase in such compounds [19,39]. Therefore, it is reasonable to assume that even in the incommensurate magnetic phase, DMI interaction continues to persist and manifests in a considerable way generating weak ferroelectric polarization. The latter may be enhanced by some other mechanism, such as, e.g., exchange striction [12] or/and oxygen spin polarization [40].

The $NdMn_2O_5$ system demonstrates the ability to generate ordered magnetic phases with slightly different $\boldsymbol{k}$ vectors depending on the temperature. Much the same situation associated with the coexistence of several magnetic phases

with similar wave vectors was observed also in DyMn$_2$O$_5$ [41]. Such a state can be realized due to the presence of several competing magnetic states. It was shown in Ref. [41] that the choice of the ground state can be obtained by a relatively small magnetic field, which reflects the proximity in the energy of the competing ground states in RMn$_2$O$_5$. In the case of NdMn$_2$O$_5$, the observed coexistence of magnetic phases can be associated with the choice of the different ground states occurring due to subtle deviations in the local environment of the manganese subsystem. Such a discrete splitting of the crystal-field levels of the 4f electrons in Nd^{3+} ions in NdMn$_2$O$_5$ under the temperatures studied here has recently been experimentally demonstrated by the infrared spectroscopy [29].

V. SUMMARY

Detailed investigation of the complex incommensurate magnetic ordering in large single crystals of NdMn$_2$O$_5$ has been performed using polarized and nonpolarized neutron-diffraction techniques. Below $T_N \sim 30.5$ K a transition to the incommensurate magnetic order (most probably plane spin-density wave modulation) with propagation vectors $\boldsymbol{k}_1 = (0.5\ 0\ k_z)$, $\boldsymbol{k}_2 = -\boldsymbol{k}_1 = (0.5\ 0\ -k_z)$ with $k_{z1} = 0.361(4)$ takes place. A few degrees below, at $T \approx 27$ K an additional incommensurate magnetic phase with similar propagation vectors k_{z2} occurs. This phase, however, shows strong deviation from sinusoidal modulation as confirmed by the observation of the $3*k_{z2}$ modulations [6]. Interestingly, just at the same temperature an independent study of the crystal field energy levels of Nd^{3+} reports the splitting of the ground-state Kramers doublet two sublevels [29], demonstrating a kind of "magnetic polarization" of the Nd ions by the Mn magnetic sublattice. Thus, distorted k_{z2} modulation may be attributed to the magnetization of Nd sublattice. This magnetic phase seems to disappear when the chiral magnetic phase called k_{z3} at lower temperature is fully formed. Significant temperature hysteresis is observed in the formation of the k_{z2} and k_{z3} phases depending on the heating or cooling sample history. Results reported here are obtained using a larger crystal of high quality and modern instrumentation with improved resolution and neutron flux in comparison to the previous studies [6,13,14] reporting somehow contradictory results about thermal evolution of incommensurate order in NdMn$_2$O$_5$. Our findings allow unifying those results, and concluding that system demonstrates the ability to generate magnetic ordered phases of different types at temperatures between 30 and 4 K. According to the SNP measurements, below $T_{Ch} \approx 21$ K

magnetic structure of NdMn$_2$O$_5$ becomes chiral and this kind of magnetic order is associated with the occurrence of the weak ferroelectricity. The resulting at lower temperature k_{z3} magnetic structure could be well approximated using general elliptic helix model. Characteristic parameters of the helix, like ellipticity (ratio between minor and major ellipse axis) and inclination of the helix plane in regard to the crystallographic *ab* plane could be calculated for different temperatures. It was shown that while heating between 4 and 18 K a reorientation transition of the helical order (interchange between the minor and major axis orientation and change in the sign on the inclination angle) happens. This reorientation may be caused by the occurrence of the k_{z2} phase attributed to the partial magnetic ordering of the Nd ions at this temperature range observed in recent work [29]. Below $\sim$5 K a commensurate antiferromagnetic order with the propagation vector (1/2 0 0) is formed on Nd subsystem; this coexists with incommensurate structure k_{z3}. It is worth noting that we did not perform explicit investigations of the magnetic ordering of Nd within this study. With the temperature increase toward T_{Ch}, magnetic ellipse on Mn becomes more stretched along the a axis. The difference in the population of the right- and left-handedness domains in the chiral magnetic phase was observed in as-grown crystal. This difference can be controlled by the external electric field in field-cooled mode. The linear dependence of the magnetic chirality from the applied electric-field strength was observed within the used field region of ± 12.5 kV/cm. Thus, strong magnetoelectric coupling for NdMn$_2$O$_5$ was demonstrated experimentally. The results are qualitatively discussed within the frame of antisymmetric DMI superexchange, concluding for a more general case that integral antisymmetric DM exchange may exist in RMn$_2$O$_5$ manganates for the structures with the symmetry lower than *Pbam*. Our experimental findings are in good agreement with the suggestion that the DMI mechanism can be responsible for the emergence of weak ferroelectricity in RMn$_2$O$_5$ multiferroics family where the weak ferroelectric phase is observed simultaneously with incommensurate magnetic chiral structure.

[1] N. Hur, S. Park, P. A. Sharma, J. S. Ahn, S. Guha, and S. W. Cheong, Nature (London) **429**, 392 (2004).

[2] Y. Noda, H. Kimura, M. Fukunaga, S. Kobayashi, I. Kagomiya, and K. Kohn, J. Phys.: Condens. Matter **20**, 434206 (2008).

[3] G. R. Blake, L. C. Chapon, P. G. Radaelli, S. Park, N. Hur, S. W. Cheong, and J. Rodriguez-Carvajal, Phys. Rev. B **71**, 214402 (2005).

[4] M. Fukunaga, Y. Sakamoto, H. Kimura, Y. Noda, N. Abe, K. Taniguchi, T. Arima, S. Wakimoto, M. Takeda, K. Kakurai, and K. Kohn, Phys. Rev. Lett. **103**, 077204 (2009).

[5] P. G. Radaelli, L. C. Chapon, A. Daoud-Aladine, C. Vecchini, P. J. Brown, T. Chatterji, S. Park, and S.-W. Cheong, Phys. Rev. Lett. **101**, 067205 (2008).

[6] S. Chattopadhyay, V. Baledent, F. Damay, A. Gukasov, E. Moshopoulou, P. Auban-Senzier, C. Pasquier, G. Andre, F. Porcher, E. Elkaim, C. Doubrovsky, M. Greenblatt, and P. Foury-Leylekian, Phys. Rev. B **93**, 104406 (2016).

[7] J. A. Alonso, M. T. Casais, M. J. Martínez-Lope, J. L. Martínez, and M. T. Fernañdez-Díaz, J. Phys.: Condens. Matter **9**, 8515 (1997).

[8] V. Polyakov, V. Plakhty, M. Bonnet, P. Burlet, L.-P. Regnault, S. Gavrilov, I. Zobkalo, and O. Smirnov, Physica B **297**, 208 (2001).

[9] I. Kagomia, S. Matsumoto, K. Kohn, Y. Fukuda, T. Shoubu, H. Kimura, Y. Nida, and N. Ikeda, Ferroelectrics **286**, 167 (2003).

[10] L. C. Chapon, G. R. Blake, M. J. Gutmann, S. Park, N. Hur, P. G. Radaelli, and S.-W. Cheong, Phys. Rev. Lett. **93**, 177402 (2004).

[11] V. Baledent, S. Chattopadhyay, P. Fertey, M. B. Lepetit, M. Greenblatt, B. Wanklyn, F. O. Saouma, J. I. Jang, and P. Foury-Leylekian, Phys. Rev. Lett. **114**, 117601 (2015).

[12] P. G. Radaelli and L. C. Chapon, J. Phys.: Condens. Matter **20**, 434213 (2008).

[13] I. A. Zobkalo, S. V. Gavrilov, N. Z. Saw Nyi, S. N. Barilo, and S. V. Shiryaev, J. Magn. Magn. Mater. **354**, 85 (2014).

[14] S. Chattopadhyay, V. Balédent, P. Auban-Senzier, C. Pasquier, C. Doubrovsky, M. Greenblatt, and P. Foury-Leylekian, Physica B **460**, 214 (2015).

[15] H. Katsura, N. Nagaosa, and A. V. Balatsky, Phys. Rev. Lett. **95**, 057205 (2005).

[16] I. A. Sergienko and E. Dagotto, Phys. Rev. B **73**, 094434 (2006).

[17] M. Fukunaga and Y. Noda, J. Phys. Soc. Jpn. **79**, 054705 (2010).

[18] S. Wakimoto, H. Kimura, Y. Sakamoto, M. Fukunaga, Y. Noda, M. Takeda, and K. Kakurai, Phys. Rev. B **88**, 140403(R) (2013).

[19] I. A. Zobkalo, S. V. Gavrilov, A. Sazonov, and V. Hutanu, J. Phys.: Condens. Matter **30**, 205804 (2018).

[20] S. V. Maleyev, Physica B **350**, 26 (2004).

[21] S. V. Shiryaev, S. N. Barilo, G. L. Bychkov, D. D. Khalyavin, A. G. Soldatov, Yu. G. Pashkevich, V. P. Gnezdilov, P. Lemmens, and G. Guentherod, in *Proceedings of the Fourth International Conference on Single Crystal Growth and Heat & Mass Transfer, Obninsk, Russia, September 24–28, 2001*, edited by V. P. Ginkin (Ministry for industry, science and technology of the Russ. Federation, Obninsk, 2001), Vol. 1, pp. 251–257.

[22] B. Pedersen, JLSRF **1**, A4 (2015).

[23] A. M. M. Schreurs, X. Xian, and L. M. J. Kroon-Batenburg, J. Appl. Crystallogr. **43**, 70 (2010).

[24] V. Huțanu, M. Meven, E. Lelièvre-Berna, and G. Heger, Physica B **404**, 2633 (2009).

[25] V. Hutanu, JLSRF **1**, A16 (2015).

[26] V. Hutanu, W. Luberstetter, E. Bourgeat-Lami, M. Meven, A. Sazonov, A. Steffen, G. Heger, G. Roth, and E. Lelièvre-Berna, Rev. Sci. Instrum. **87**, 105108 (2016).

[27] V. Hutanu, M. Meven, S. Masalovich, G. Heger, and G. Roth, J. Phys.: Conf. Series **294**, 012012 (2011).

[28] J. Rodriguez-Carvajal, Physica B **192**, 55 (1993).

[29] S. Mansouri, S. Jandl, M. Balli, P. Fournier, B. Roberge, M. Orlita, I. A. Zobkalo, S. N. Barilo, and S. V. Shiryaev, Phys. Rev. B **98**, 205119 (2018).

[30] P. J. Brown and T. Chatterji, *Neutron Scattering from Magnetic Materials* (Elsevier Science, Amsterdam, 2006), pp. 215–244.

[31] Yu. A. Izyumov and R. P. Ozerov, *Magnetic Neutron Diffraction* (Nauka, Moscow, 1966; Plenum, New York, 1970).

[32] M. Kenzelmann, A. B. Harris, S. Jonas, C. Broholm, J. Schefer, S. B. Kim, C. L. Zhang, S.-W. Cheong, O. P. Vajk, and J. W. Lynn, Phys. Rev. Lett. **95**, 087206 (2005).

[33] T. Arima, A. Tokunaga, T. Goto, H. Kimura, Y. Noda, and Y. Tokura, Phys. Rev. Lett. **96**, 097202 (2006).

[34] O. Prokhnenko, R. Feyerherm, E. Dudzik, S. Landsgesell, N. Aliouane, L. C. Chapon, and D. N. Argyriou, Phys. Rev. Lett. **98**, 057206 (2007).

[35] F. Keffer, Phys. Rev. **126**, 896 (1962).

[36] A. S. Moskvin and I. G. Bostrem, Fiz. Tverd. Tela **19**, 2616 (1977) [Sov. Phys. Solid State **19**, 1532 (1977)].

[37] P. W. Anderson, in *Magnetism*, edited by G. T. Rado and H. Suhl (Academic Press, New York, 1963), Chap. 2, pp. 25–83.

[38] L. M. Volkova and D. V. Marinin, J. Phys.: Condens. Matter **21**, 015903 (2009).

[39] H. Kimura, S. Kobayashi, Y. Fukuda, T. Osawa, Y. Kamad, Y. Noda, I. Kagomiya, and K. Kohn, J. Phys. Soc. Jpn. **76**, 074710 (2007).

[40] T. A. W. Beale, S. B. Wilkins, R. D. Johnson, S. R. Bland, Y. Joly, T. R. Forrest, D. F. McMorrow, F. Yakhou, D. Prabhakaran, and A. T. Boothroyd, and P. D. Hatton, Phys. Rev. Lett. **105**, 087203 (2010).

[41] W. Ratcliff II, V. Kiryukhin, M. Kenzelmann, S.-H. Lee, R. Erwin, J. Schefer, N. Hur, S. Park, and S.-W. Cheong, Phys. Rev. B **72**, 060407(R) (2005).